Proving the viability of an electrochemical process for the simultaneous extraction of oxygen and production of metal alloys from lunar regolith

Bethany A. Lomax,[a] Melchiorre Conti,[b] Nader Khan,[b] Nick S. Bennett,[c] Alexey Y. Ganin,[a] and Mark D. Symes*[,a]

[a] *WestCHEM, School of Chemistry, University of Glasgow, Glasgow, G12 8QQ, United Kingdom*

[b] *Metalysis, Advanced Manufacturing Park, Rotherham, S60 5FS, United Kingdom*

[c] Institute of Mechanical, Process and Energy Engineering, *Heriot-Watt University, Edinburgh, EH14 4AS, United Kingdom*

**Email: mark.symes@glasgow.ac.uk*

Abstract: The development of an efficient process to simultaneously extract oxygen and metals from lunar regolith by way of in-situ resource utilisation (ISRU) has the potential to enable sustainable activities beyond Earth. The Metalysis-FFC (Fray, Farthing, Chen) process has recently been proven for the industrial-scale production of metals and alloys, leading to the present investigation into the potential application of this process to regolith-like

materials. This paper provides a proof-of-concept for the electro-deoxidation of powdered solid-state lunar regolith simulant using an oxygen-evolving SnO_2 anode, and constitutes the first in-depth study of regolith reduction by this process that fully characterises and quantifies both the anodic and cathodic products. Analysis of the resulting metallic powder shows that 96% of the total oxygen was successfully extracted to give a mixed metal alloy product. Approximately a third of the total oxygen in the sample was detected in the off-gas, with the remaining oxygen being lost to corrosion of the reactor vessel. We anticipate, with appropriate adjustments to the experimental set-up and operating parameters, to be able to isolate essentially all of the oxygen from lunar regolith simulants using this process, leading to the exciting possibility of concomitant oxygen generation and metal alloy production on the lunar surface.

Keywords: In-situ resource utilisation, ISRU, FFC-Cambridge process, Metalysis-FFC process, lunar regolith, oxygen extraction, metal production

1. Introduction

Human exploration and habitation of the Moon and other nearby planetary bodies are goals that have long fascinated scientific and public imagination. Sourcing resources locally will likely be essential for sustainable, long-duration activities in space (Anand et al. 2012). Such in-situ resource utilisation (ISRU) could significantly reduce the payload mass that would need to be launched from Earth, thus reducing mission cost and the risk to human crews by providing them with the tools to meet their needs from the local environment (Sanders and Larson, 2012).

For extended missions to the lunar surface (and beyond), oxygen will undoubtedly be one of the most valuable resources. Firstly, it will be useful for life support, in the form of a breathable atmosphere, and secondly for propellant, as liquid oxygen is the largest mass component of many bipropellant rockets. In-space refuelling would enable not only lunar and deep-space exploration, but also sustainable activities in cis-lunar space. It is more energy efficient to transport propellant from the Moon to satellites in low-Earth orbit (LEO) and geostationary orbit (GEO) than it is to transport such materials from the Earth's surface on account of Earth's deep gravitational well (Crawford, 2015). While evidence is mounting for ice deposits in permanently shadowed craters at the lunar poles (Li et al. 2018), their potential as a viable source of oxygen and hydrogen cannot be confirmed until knowledge gaps relating to form, quantity, and accessibility of deposits are addressed (Carpenter et al. 2016).

In contrast, a thick layer of unconsolidated regolith covers the entire lunar surface, making it an assured feedstock for resource extraction. Based on analyses of various Luna and Apollo samples, it is known that oxygen is the most abundant element in lunar regolith, accounting for 40 - 45% by mass (McKay et al. 1991). However, this oxygen is chemically bound in the regolith material as oxides, in the form of minerals and amorphous glass, and is therefore unavailable for immediate use. The extraction and processing of oxygen from the lunar regolith will likely be essential to enabling future exploration and habitation of the Moon (Taylor and Carrier, 1993). Moreover, development of a process to reduce lunar regolith that allows for the simultaneous extraction of oxygen and production of useful metals and alloys for lunar infrastructure would be highly beneficial.

Numerous strategies for extracting oxygen from regolith material on the lunar surface have been proposed; summaries of such processes can be found in previous publications (Taylor and Carrier, 1993; Schrunk et al. 2007; Schwandt et al. 2012a). Some of the more well-researched processes are the chemical reduction of regolith-derived iron oxides either with hydrogen, followed by the electrolysis of water (Gibson et al., 1994; Allen et al. 1996; Li et al. 2012; Sanders and Larson, 2012), or alternatively with methane, which would require a further methane-reforming step and the electrolysis of water (Friedlander, 1985). These processes operate at ~900 °C, utilising a low-risk solid-gas interaction, but are low yielding (1-3%) and heavily dependent on feedstock composition and beneficiation. 'Yield' in this context is defined as weight of oxygen extracted divided by total weight of regolith processed. The carbothermal reduction of molten regolith at ~1600 °C (also requiring subsequent methane-reforming and electrolysis steps; Rosenberg et al., 1992; Gustafson et al., 2006; Balasubramaniam, 2010; Sanders and Larson, 2012), and the direct electrolysis of molten regolith at >1600 °C (Colson and Haskin, 1992, 1993; Vai et al. 2010; Sirk 2010; Wang et al. 2011; Schreiner 2016), are less feedstock-dependent and higher yielding (theoretically 10-20% and 20-30% respectively), but require the handling of molten regolith at extreme temperatures. Research has also been conducted into the use of molten fluoride salts as a flux to dissolve lunar regolith oxide simulants and related silicate rocks at 960 - 1250 °C, and hence to extract a mixed alloy electrochemically; however, these processes rely on the solubility of the various oxides and the efficacy in terms of oxygen yield has not been quantified (Kesterke 1970; Liu et al. 2017).

Against this backdrop of possible oxygen extraction techniques requiring multi-step chemical processes, specific feedstock compositions, and/or extreme temperatures, an attractive

alternative is provided by direct electro-deoxidation of solid regolith. The FFC (Fray, Farthing, Chen)-Cambridge process involves the solid-state electrochemical reduction of metal oxides to metals in molten salt ($CaCl_2$) at temperatures of around 900 °C (Fray et al., 1999; Chen et al., 2000). A schematic of a typical FFC-Cambridge electrolysis cell is shown in Figure 1, along with the half-equations for the reactions occurring at the anode and cathode. In the terrestrial system, a graphite anode facilitates the removal of oxygen from the system in the form of CO_2 and CO; in the lunar context, an oxygen-evolving anode could be used to produce oxygen directly. In contrast to the lunar oxygen extraction processes listed above, electro-deoxidation in molten salt electrolyte offers a number of benefits. This process can theoretically reduce all lunar minerals and oxides, which removes any constraints on regolith composition (and therefore the locations suitable for oxygen extraction on the Moon), and vastly reduces the excavation and beneficiation requirements. As the FFC-Cambridge process is an electrochemical process that operates without having to melt the material being reduced, much lower temperatures (~900 °C) are required to reduce lunar silicates than by chemical reduction (i.e. with carbon at ~1600 °C), or electrolysis of molten regolith (>1600 °C). Furthermore, an optimised FFC-Cambridge electrolyser on the Moon, with closed-loop salt recycling and a reusable inert anode, would require only regolith and a source of electricity to generate oxygen and reduced metal alloys. Finally, the molten salt electrolyte could also provide a means to store energy during the lunar night, increasing the usefulness of the payload weight (Hasnain, 1998).

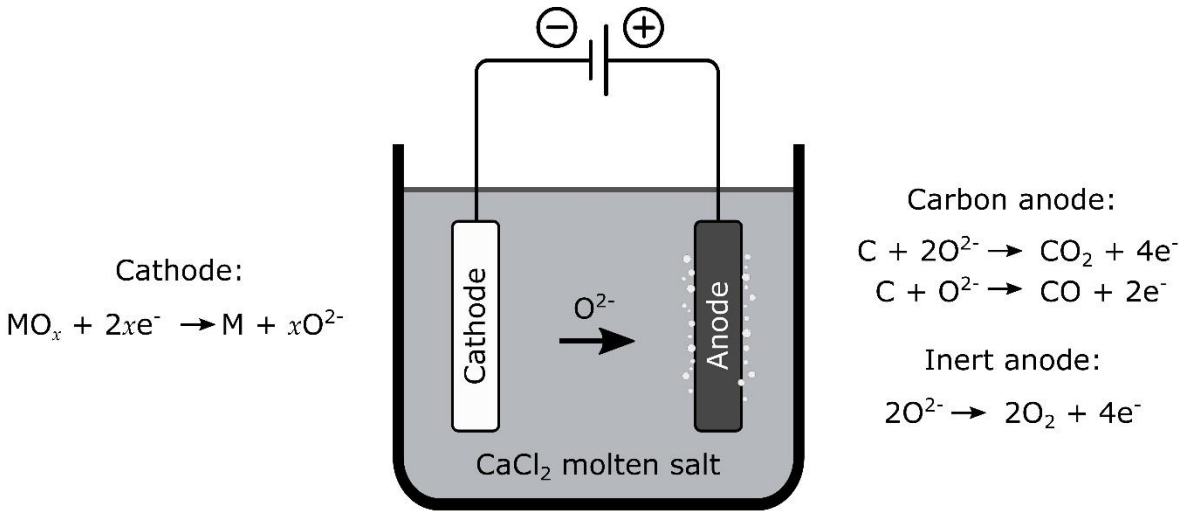

111

112 **Figure 1:** A diagram showing the basic concept of the FFC-Cambridge process, whereby a
113 metal oxide (MO_x) is reduced to the corresponding metal with the co-generation of CO/CO_2
114 (at a graphite anode) or O_2 at an inert anode.

115

116 In the past decade, Metalysis (a UK-based company) have successfully scaled-up the FFC-
117 Cambridge technology from research and development (R&D) scale Generation 1 cells, with
118 a further three generations designed, commissioned, and in operation. Developments in pre-
119 forming, electrolysis, salt management, and post processing have turned a laboratory-based
120 technology into an end-to-end commercial process (Mellor and Doughty, 2016). As of 2018,
121 titanium and tantalum metal production has been developed at an industrial scale, and the
122 production of many other metals and alloys has also been proven (Figure 2). More recently,
123 the production of intermetallics of aluminium and scandium has been scaled-up to industrial
124 production. As a solid state-to-solid state process, the Metalysis-FFC technology is also
125 uniquely placed to create high entropy alloys (containing three to seven different elements in
126 equimolar amounts), often combining metals that otherwise could not be mixed on account
127 of the large disparities in phase change behaviour (Ellis and Doughty, 2017). As seen in Figure

2, the Metalysis-FFC electro-deoxidation process is well placed to reduce and extract oxygen from all the major components of lunar regolith, while creating useful alloys as by-products.

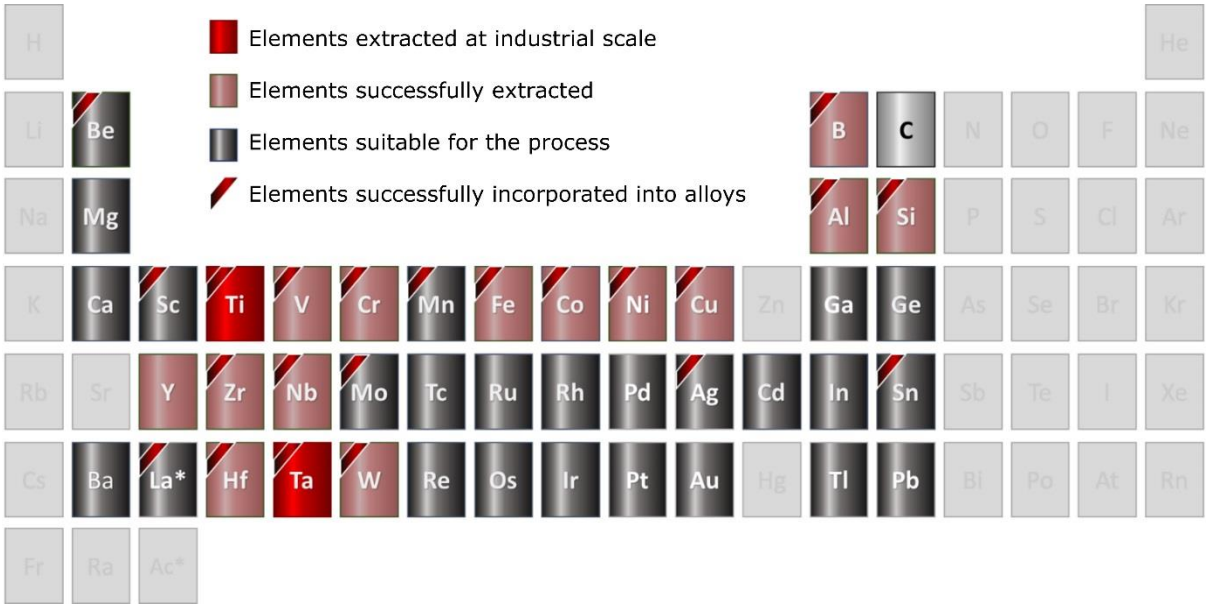

Figure 2: The status of the extraction and commercialisation of various elements with the Metalysis-FFC process as of 2018.

When considering the application of this process on the lunar surface, recent developments offer much promise. Metalysis routinely produce pure metals and alloys that are required by commercial specifications to have oxygen contents <0.5 wt.%, which exceeds the ISRU requirements to make lunar oxygen extraction sustainable. A single Generation 4 cell could produce around 6 tonnes of oxygen per year from a regolith feedstock that contains ~40% oxygen by weight, and with Generation 5 cells already in the feasibility study stage, a highly automated set up has been designed (Vaughan and Conti, 2017). In terms of salt reusability, Metalysis' production units run continuously throughout the year, with the crucible and electrolyte salt being used for the entire production campaign. The ratio between electrolyte salt and metal oxide feedstock that is currently employed has been optimised for the

production of ultra-pure metals in a terrestrial setting (where reactor size is not a significant issue). This ratio could be readily altered so as to use less electrolyte salt and make the payload more compact if it was decided that the purity of the deoxidised by-product was less important than the size or weight of the reactor.

A previous NASA-funded study (undertaken in 2004) investigated the applicability of the FFC-Cambridge process for the electrolysis of lunar ilmenite, termed the Ilmenox process (Schwandt et al. 2012a). At the time of this previous work, the development of the FFC-Cambridge process was still in its early stages and had only been proven at a laboratory scale. In their study, Schwandt et al. (2012a, 2012b) showed that oxygen could be obtained by the FFC-Cambridge electrolysis of pellets of the mineral ilmenite at 900 °C using an inert anode (either doped tin oxide (Kilby et al., 2010) or a calcium titanate/calcium ruthenate mixture (Jiao et al., 2009; Jiao and Fray, 2010)). The authors also described the electro-generation of oxygen from pellets of the lunar simulant JSC-1. However, for both the ilmenite and JSC-1 experiments, the reduced cathode products were not analysed in any great detail save for confirmation of their metallic (reduced) nature. Moreover, the total oxygen removed from the regolith-like materials as a percentage of that available was not quantified. It seems, therefore, that a more detailed investigation of the FFC-Cambridge process for the generation of oxygen and reduced metallic species from simulant lunar regolith is warranted in order to take advantage of recent process developments and to gauge the potential of solid-state electro-deoxidation for the reduction of all lunar regolith components (not just ilmenite) in the powdered form.

Herein, we provide proof-of-concept that the lunar regolith simulant JSC-2A can be reduced from a loose powder bed under Metalysis-FFC conditions, in contrast to the previous ilmenite-focussed study that used pressed and sintered tiles. The final oxygen content in the reduced product shows that almost all (96%) of the total oxygen has been removed in this fashion. Around a third of the oxygen that is liberated can be detected in the headspace of the reactor by mass spectrometry. The rest appears to react with the containment vessel to give corrosion products (a side reaction that we hope to minimise in future studies by employing an improved reactor design). Hence, we believe that with proper optimisation of our apparatus it should be possible to extract essentially all of the oxygen contained within the regolith simulant as O_2 gas. The reduced solid metallic products are rich in alloys of aluminium and iron, and also contain silicon, calcium, magnesium and titanium in appreciable quantities. However, the overall composition appears to be depleted in silicon and magnesium relative to the starting material. A hypothesis is proposed for the relative lack of these elements, which, if proven, could lead to the intriguing possibility that specific metals or alloys could be siphoned off directly from the reactor in reasonable purity for use on the Moon. The metallic product is shown to be largely devoid of sodium and potassium, making it highly akin to the type of material that might be obtained from genuine regolith (which is poor in both of these elements). On the basis of these preliminary results, we conclude that there seems to be no fundamental reason as to why this process could not operate effectively on the lunar surface, giving essentially 100% oxygen extraction and producing useful highly-reduced metals and alloys as by-products.

2. Materials and Methods

2.1 Materials: The JSC-2A simulant used in this study was supplied by Zybek Advanced Products (ordered mid-2017). $CaCl_2$ salt (analytical grade) was supplied by Total Lab and CaO (96% pure) was supplied by Acros. A doped tin oxide anode (SnO_2 with 1% Sb_2O_3 and 0.45% CuO) was used for all experiments and was supplied by Dyson Technical Ceramics.

2.2 Metalysis-FFC Electrolysis Cell: The electrolysis cell consisted of an alumina crucible inside a stainless steel (SS) retort, sealed with a water-cooled lid. The cell lid contained feedthroughs for three electrode rods, a thermocouple, a viewport, an argon line inlet to provide an inert atmosphere and remove process gases, and an outlet to a mass spectrometer. A SS basket was lined with SS mesh, and attached to two cathode rods. A SnO_2 anode was attached to the end of the anode rod and positioned centrally relative to the cathode basket. Resistance checks were performed to ensure adequate connection between all components. The electrolysis cell set-up is shown in Figure 3.

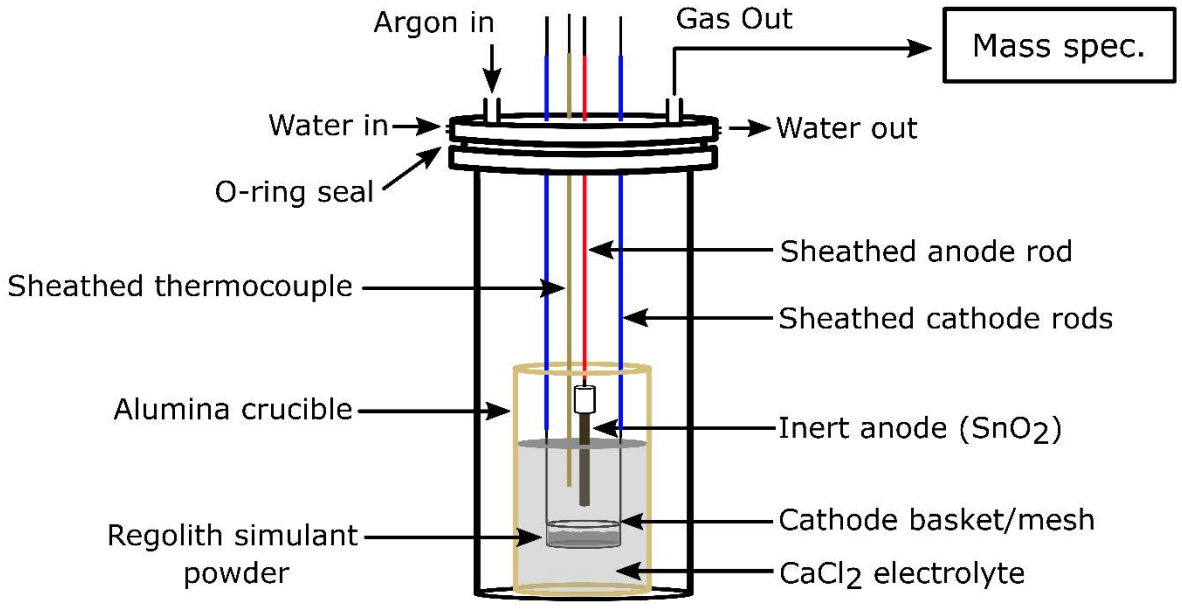

Figure 3: The experimental set-up of the electrolysis cell for reductions of powdered regolith simulant.

2.3 Electrolysis Experiments: Reduction experiments were carried out using 30 g of JSC-2A lunar regolith simulant (maximum grain size 1 mm) sieved to >53 µm to ensure all powdered material was contained by the 50 µm cathode basket mesh. The crucible containing 1600 g pre-dried $CaCl_2$ salt with a starting CaO concentration of approximately 0.4wt.%, as measured by acid-base titration, was placed in the retort. The cell was sealed with the cathode basket (containing starting material), anode, and thermocouple all sitting above the salt line, and the temperature was ramped up to 950 °C (10 °C/min). The cathode, anode, and thermocouple were then lowered into the molten salt. The electrolyte was sampled once the temperature had reached 950 °C and again after the experiment was complete and the salt had cooled and solidified.

The current was ramped up at a rate of 0.25 A/min until 4 A was reached. Reduction experiments were then performed at a constant current of 4 A. Full reduction experiments were run for as long as possible to ensure complete reduction (45 – 52 hours in practice). Partial reduction experiments were run for 16 or 26 hours. Mass spectrometry was used to record the O_2, HCl, Cl_2, CO_2, CO and H_2O concentrations in the off-gas.

2.4 Post-electrolysis Processing of Cathode Materials: Following electrolysis, the cathode basket was removed from the salt and left to cool under argon. It was then soaked in water to dissolve the salt and separate all the products from the basket. The product material was lightly ground and washed with water in a mortar and pestle until the wash water ran clear. The product was then transferred to a 0.45 µm filter and washed with water until no salt remained; this was confirmed using a conductivity meter. The resulting powder was then oven-dried overnight.

Magnetic material was removed from the dried product; the magnetic fraction was made up of SS mesh material and other non-product material from the reactor. The powdered product material was then separated by mechanical sieve to give fractions of the following sizes: 0-75 µm, 75-150 µm, 150–300 µm, and >300 µm. Following standard procedures, confirmed by subsequent analysis, the finest fraction was discarded.

2.5 Characterisation: The oxygen content of the solid samples was measured with an Eltra ON-900 oxygen/nitrogen analyser. Powdered samples were mounted for SEM in pressed Struers Polyfast conductive Bakelite resin and polished using a Struers TegraPol-11 with SiC paper, diamond paste, and a silica polishing suspension. SEM-EDX (scanning electron microscopy with energy dispersive x-ray) analysis was carried out using a Carl Zeiss Sigma Analytical SEM with an acceleration voltage of 20 kV and an Oxford Instruments EDX detector operated through Aztec Microanalysis software. Back-scattered electron (BSE) images and EDX elemental mapping (EM) were used to analyse phase composition. XRD analysis was performed on a Panalytical X'Pert PRO MPD diffractometer with a Cu $K\alpha_1$ radiation source in either a flatplate spinner or zero-background configuration in Bragg-Brentanno reflection geometry. Samples were ground with a mortar and pestle prior to XRD analysis. Inductively coupled plasma mass spectrometry (ICP-MS) was used to analyse the $CaCl_2$ electrolyte samples.

3. Results and Discussion

3.1 Characterisation of Starting Materials

JSC-2A lunar regolith simulant, a replica of previous simulant version JSC-1A, is a ground volcanic tuff originating from the San Francisco volcano field near Flagstaff, Arizona (Ray et

al. 2010). The major element composition as specified by the manufacturers is given in Table 1, and shows it to consist chiefly of silicon, aluminium, iron, magnesium and calcium oxides, with small but significant quantities of other elements also present. Of course, these elements do not exist as pure oxides in the simulant, but rather as mineral and amorphous phases that will influence reduction behaviour.

Hill et al. (2007) measured the abundance of the main phases in JSC-1A as 49.3% volcanic glass, 38.8% plagioclase feldspar, and 9% olivine with minor amounts of other minerals such as chrome spinel, sulfide, titanomagnetite, quartz, and pyroxene. The phase analysis of JSC-2A (>53 µm) using EDX elemental mapping (Figure 4) shows it to contain similar proportions of these main phases to those identified by Hill et al. (2007). The element maps overlaid to create this image are shown in Supplementary Figure S1 (see Appendix). The compositions found by spot EDX analysis of the two main minerals in JSC-2A are given in Figure 5 and show reasonably tight grouping with a plagioclase composition of An_{60-72} (labradorite) and an olivine composition of Fo_{65-80} (forsterite (ferroan)). The average composition of the volcanic glass in JSC-2A is relatively similar to the bulk composition. The diffraction pattern of JSC-2A (>53 µm), shown in Figure 9, confirms the two dominant crystalline phases are labradorite (average assigned composition $Ca_{0.66}Na_{0.34}Al_{1.66}Si_{2.34}O_8$) and forsterite (ferroan) (average assigned composition $Mg_{1.44}Fe_{0.56}SiO_4$).

Table 1: Bulk oxide composition of lunar regolith simulant JSC-2A as given by the suppliers (Zybek Advanced Products).

Oxide	Wt.%
SiO_2	46-49
TiO_2	1-2
Al_2O_3	14.5 – 15.5

Fe_2O_3	3-4
FeO	7 – 7.5
MgO	8.5 – 9.5
CaO	10 – 11
Na_2O	2.5 – 3
K_2O	0.75 – 0.85
MnO	0.15 – 0.20
Cr_2O_3	0.02 – 0.06
P_2O_5	0.6 – 0.7

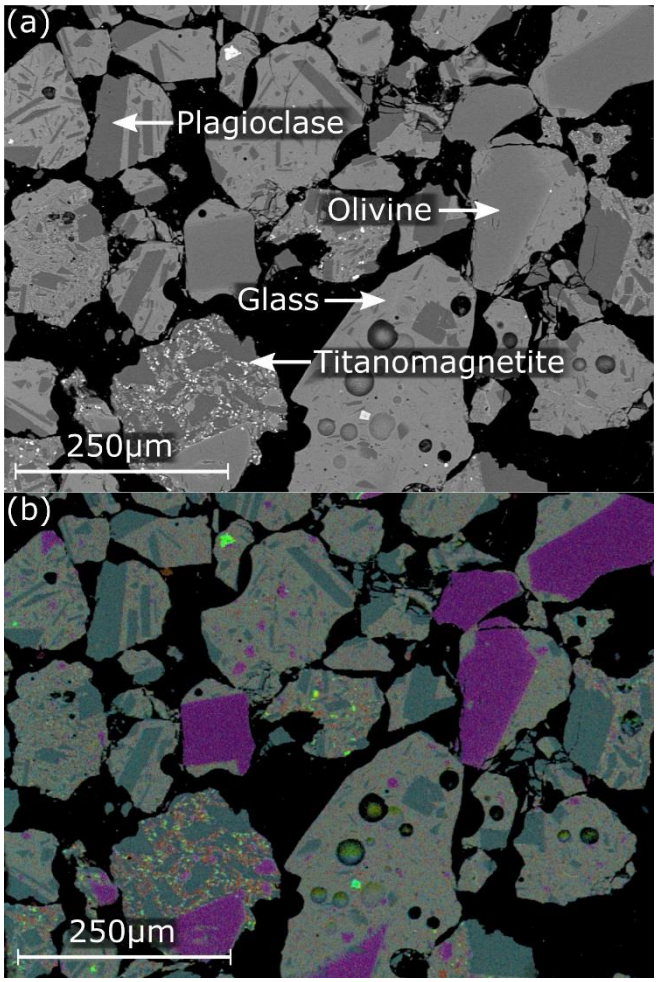

Figure 4: The BSE image (a), and element map (b) of JSC-2A simulant (sieved to >53 µm) showing the main phases to be plagioclase (blue) and olivine (purple) minerals within a glass (grey) matrix. Small spots of titanomagnetite (green) and pyroxene (orange) can also be seen.

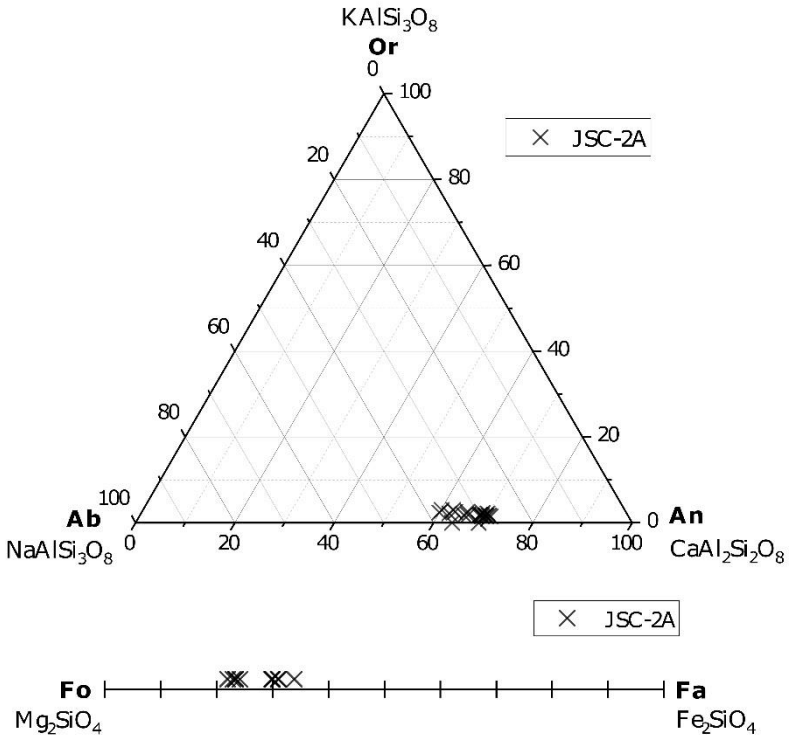

Figure 5: Compositional diagrams for the plagioclase (top) and olivine (bottom) in the JSC-2A starting material.

As a simulant material, JSC-2A constitutes a reasonable approximation to lunar regolith composition, meaning that it is valid to use JSC-2A to draw conclusions about the general applicability of the Metalysis-FFC process to lunar regolith. Furthermore, the wide usage of JSC-1A in ISRU experiments makes JSC-2A, as a replica from the same natural source, the simulant of choice for comparison to a range of studies. While the JSC simulants can be used to prove general applicability to regolith-like material, conclusions about specific lunar locations (i.e. mare vs. highlands) will not be included in the present work as the bulk chemical compositions of the JSC range of simulants show them to be atypical of either the mare or highland regions, with chemistry similar to select Apollo 14 soils whose composition falls in between the two groupings and only represents 2-3% of the lunar surface (Taylor et al. 2016).

Understanding the individual phases present in JSC-2A and how they behave throughout the reduction process does, however, allow for comparison to equivalent or similar lunar phases. The volcanic glass is a reasonable approximation for the high glass content of lunar agglutinates and the olivine composition measured here falls within the range of lunar olivine (Papike et al. 1991). The plagioclase composition is too Na-rich, compared with lunar plagioclase (typically An90-100), an issue common to most terrestrial simulants due to the lunar crust being comparatively depleted of alkali metals (Canup et al. 2015). However, this mineral can still be seen as a useful proxy for investigating general plagioclase reduction. The inclusion of iron oxides in the form of small titanomagnetite grains throughout the glass matrix may emulate the reduction behaviour of lunar ilmenite and/or the alloy forming-behaviour of lunar nanophase iron.

3.2 Detection and Quantification of Oxygen during Electro-deoxidation of JSC-2A

Electrolysis was conducted at a fixed current of 4 A using the cell configuration shown in Figure 3 for 52 h. Figure 6 shows the rate of removal of oxygen from 30 g powdered simulant JSC-2A (sieved to >53 µm) during electrolysis, as measured by in-line mass spectrometry (black trace). The calculated background oxygen concentration (~50 ppm) has been subtracted from all oxygen detection data. The corresponding potential *vs.* time curve and mass spectrometry data is shown in Supplementary Figure S2 and S3 and shows that the period in Figure 6 (44.0 – 46.6h) during which no oxygen is detected corresponds to a period during which no current was being passed. This was due to the anode partially breaking and losing contact with the electrolyte. At t = 46.6 hours, the anode was lowered back into the salt and electrolysis continued. While the anodes used in this study do indeed facilitate the

direct production of O_2, a number of mechanical issues were identified, which will be addressed in future work. The cumulative oxygen detected as a percentage of the total oxygen content of the starting material is shown by the red dashed line in Figure 6. After 52 h (~49 h running time), the total oxygen detected corresponded to around 34% of the oxygen present in the starting material (4.48 g of oxygen from a 30 g sample of regolith simulant).

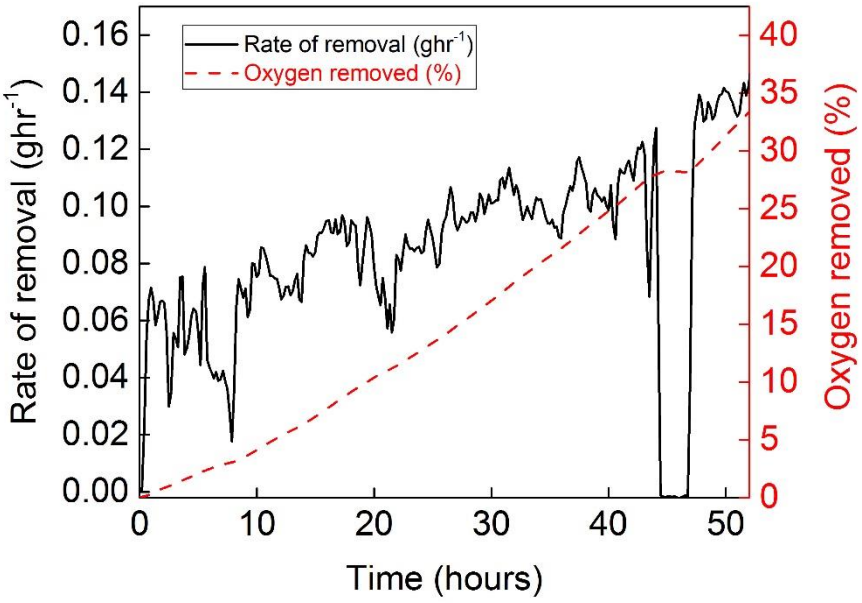

Figure 6: The rate of oxygen removal, calculated from mass spectrometer data, and the percentage of oxygen detected as a function of the total oxygen content of the starting material. The period of no oxygen removal after 44 hrs corresponds to the anode losing contact with the electrolyte.

3.3 Quantification of Oxygen in the Solid Product:

Following electrolysis, the reduction products were washed with water to remove electrolyte salts and sieved to give various size fractions for subsequent analysis. The appearance of the metallic powder produced from the reduction of JSC-2A is shown in Figure 7. Table 3

demonstrates the mass distribution of metallic products with sieve diameters in excess of 75 µm obtained from this reduction, giving an overall solid product yield of 64% (assuming complete reduction of the starting materials to metals in their zero oxidation state). As discussed below, we suspect that some of the metallic material may have been expelled from the cathode during the reduction, thereby reducing the mass of the remaining product. Doubtless, this yield could also be greatly improved in future experiments by refining the experimental and post-electrolysis processing procedures. Oxygen analysis of the reduced simulant gives a combined average of only 3.1 wt.% oxygen remaining. This equates to a potential "oxygen extraction/recovery %" (mass of oxygen extracted ÷ mass of available oxygen) of 96%. Based on the oxygen content of JSC-2A an "oxygen yield %" (mass of oxygen extracted ÷ mass of regolith) of 42% was obtained, which can be compared to the oxygen yields of other extraction methods discussed herein. In our case, the percentage oxygen extracted may be higher (if uncollected material was lost in the metallic form), or lower (if the uncollected material was lost as oxide before it could be reduced). Therefore, we believe that the oxygen extraction yield based on the collected material is a reasonable approximation to that which the process is capable of extracting.

Moreover, as Table 2 shows, the percentage of oxygen in the solid product material increases as the diameter of the material decreases (i.e. as the surface area to volume ratio increases). This is the opposite trend to that which would be expected to hold during reduction whereby larger grain sizes would be expected to take longer to fully reduce, suggesting that much of this oxygen content arises as a result of re-oxidation of the surface of reduced material during post-electrolysis processing of the cathode product. Alternate methods of post-electrolysis processing will be explored in future work to mitigate this potential surface re-oxidation prior to analysis. The mass of the fraction below >75 µm accounted for only 9% of the total material

isolated after post-electrolysis processing and was found by SEM-EDX analysis to contain a significant proportion of material not derived from the regolith simulant, but instead emanating from other sources in the reactor, such as the anode. The fine fraction in Metalysis-FFC powder-to-powder reductions is typically discarded for similar reasons.

The primary reason for the discrepancy between the oxygen gas detected by mass spectrometry during bulk electrolysis and the oxygen content of the reduced solid products lies in the fact that at these temperatures the oxygen gas that is produced reacts with the reaction vessel itself and so a significant amount is lost to corrosion. To some extent, this is not surprising as the reactors in use were designed for the traditional FFC-Cambridge process, which produces CO and CO_2 rather than O_2 (which is significantly more oxidising). Hence, our in-line oxygen detection serves more as a proof-of-principle that oxygen gas can indeed be directly generated through this process; quantitative recovery of this oxygen will require different reactor vessel materials to be employed. In light of this, we contend that the low oxygen content of the solid products of the reduction reaction gives a better indication of the potential for oxygen extraction than the amount of oxygen gas detected with the current apparatus. Similarly, the rate of oxygen extraction shown in Figure 6 does not necessarily reflect the rate of reduction. Analysis of the simulant after 16 hours of electrolysis under the same conditions shows that ~76% of the total available oxygen had already been extracted. Comparing this to the 96% oxygen extraction achieved after ~50 hours clearly shows that the reduction proceeds more rapidly in its early stages. This trend is also reflected in the Faradaic efficiency of 23% for the more complete reduction after ~50 hours, compared with 49% for the 16-hour partial reduction (based on oxygen remaining in the reduced simulant product). With optimisation of the electrolysis parameters for oxygen production rather than metal production in future work, we anticipate that the current efficiencies can be increased.

However, as they stand, they are in a similar range to the current efficiencies achieved in traditional FFC-Cambridge processing (Schwandt, 2010).

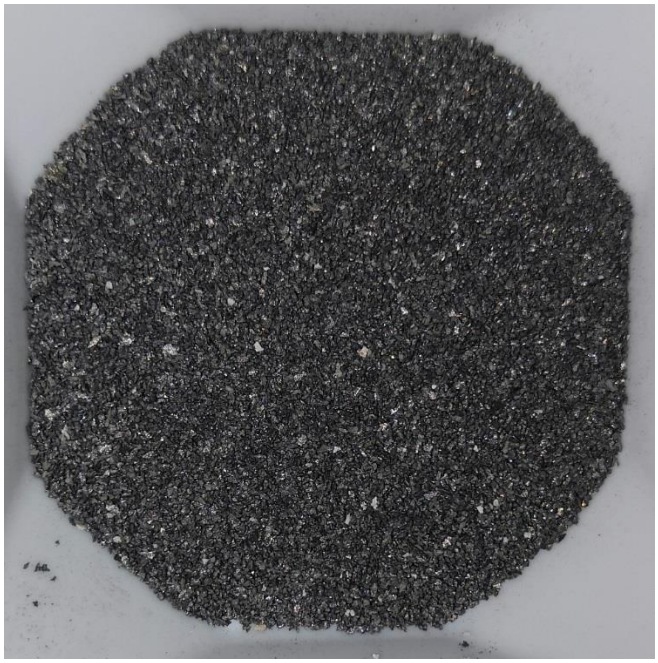

Figure 7: An example of the 150 – 300 µm fraction of the metallic powder produced by the reduction of JSC-2A (4 A, 950 °C, doped-SnO_2 anode, 49 hrs).

Table 2: The mass and oxygen content (wt. %) of a reduced product by size fraction showing that the percentage of oxygen remaining in the reduced product decreases as grain size increases.

Size fraction	Mass (g)	Oxygen (wt.%)
75-150 µm	1.66	5.9
150-300 µm	3.21	3.2
300+ µm	5.94	2.3

3.4 Characterisation of Metallic Products

398 The powder X-ray diffraction pattern of the starting material JSC-2A (>53 µm) can be assigned
399 to two main crystalline phases, labradorite and forsterite (ferroan) minerals. By comparison,
400 the diffraction pattern of the cathode product (a proportionate mixture of all >75 µm
401 fractions) reveals a dramatic change in peaks, clearly indicating that the reduction process
402 leads to a significant change in phase composition (Figure 8). The XRD pattern of the reduced
403 product shows multiple peaks that can be assigned to various metal alloys, while no peaks
404 were identified that can be assigned unambiguously to oxides or minerals. As far as powder
405 X-ray diffraction can ascertain, therefore, it appears the material has been fully reduced. The
406 main constituents that can be identified by X-ray diffraction are two Al/Fe alloys (with small
407 variations in the Al:Fe ratio accounting for the slight splitting of the main peaks), an Al/Fe/Si
408 alloy, and a Ca/Al/Si alloy. Due to the complex composition of the natural starting material,
409 and the inevitable complexity of the product resulting from reduction of this starting material,
410 assignment of minor phases in the diffraction pattern is challenging.
411

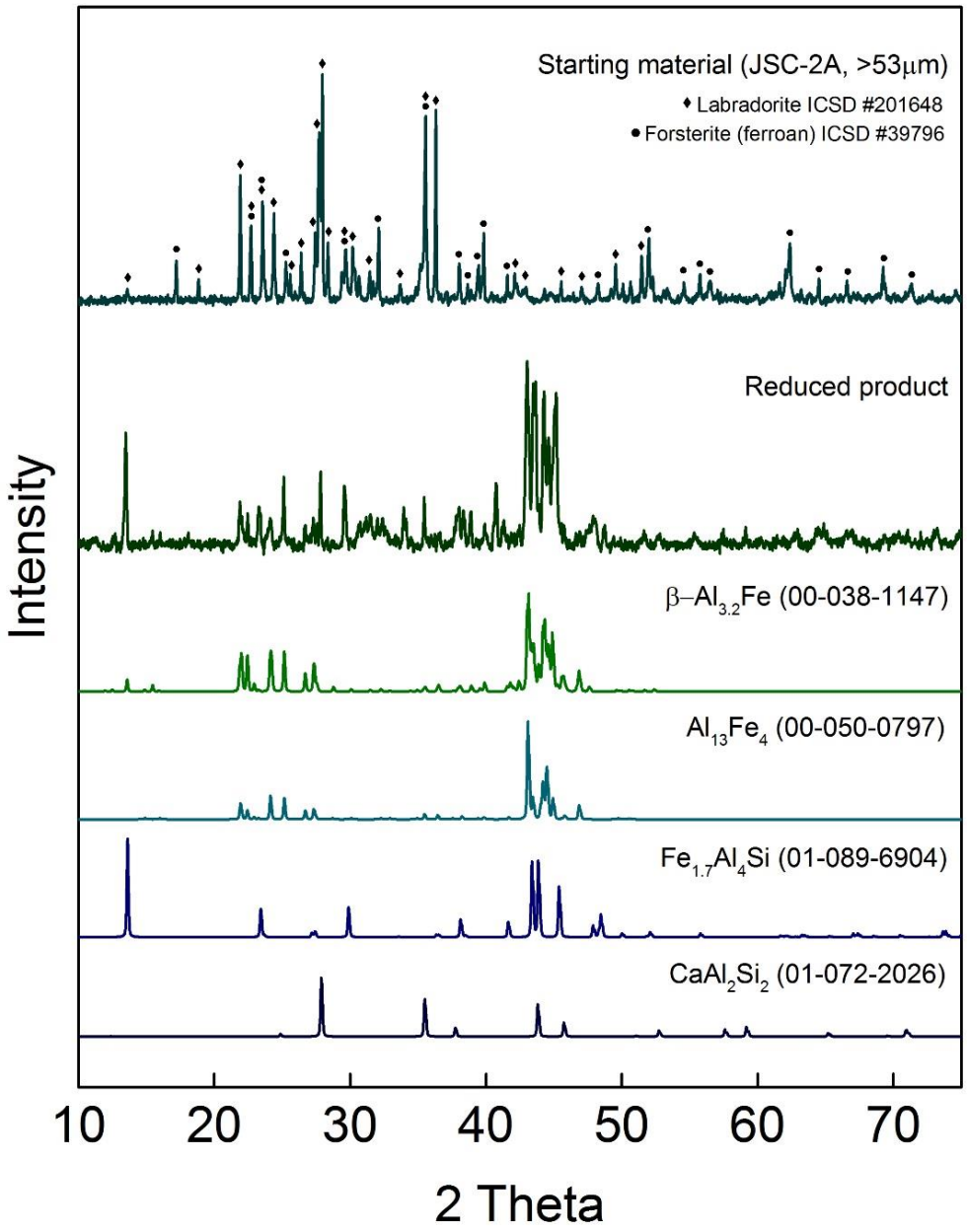

412

413 **Figure 8:** Powder XRD (CuK_a) pattern of the starting material (top), comprised primarily of
414 labradorite ($Ca_{0.66}Na_{0.34}Al_{1.66}Si_{2.34}O_8$) and forsterite (ferroan) ($Mg_{1.44}Fe_{0.56}SiO_4$); and the
415 diffraction pattern of the mixed alloy product (4A, 950 °C, doped-SnO_2 anode, 49 hrs) with
416 the simulated diffraction patterns from the major phases identified shown below for
417 comparison (PDF (Powder Diffraction File) database number in brackets). Both experimentally
418 obtained diffraction patterns have been baseline-corrected.

Greater insight into the nature of the solid products of reduction can be obtained by SEM/EDX. Analysis of these data show the cathode product to be fully reduced metal grains containing metal alloys. In particular, the products are dominated by an Al/Fe alloy (approximately 3:1 Al to Fe ratio), sometimes with the inclusion of up to 10% silicon, which is in good agreement with the powder X-ray diffraction data. Another reoccurring phase identified by EDX is an Fe/Si alloy, that also regularly contains Ti and/or Al in significant amounts, most commonly situated inside a particle of the previously mentioned Al/Fe alloy with distinct phase boundaries. The distinction between the titanium and non-titanium variation is likely due to whether the grain initially contained titanomagnetite. We expect that due to the large number of compositional permutations of these four elements, they each account for only minor reflections in the XRD pattern and, therefore, have not been assigned in Figure 8. The final phase that can be seen in a large number of particles is a Ca/Si/Al phase, sometimes with the inclusion of Mg. This phase, without the Mg component, is consistent with the XRD diffraction analysis. Taken together, the alloys discussed up to this point appear to account for the vast majority of the reduced material.

The phase map in Figure 9 shows an example of a grain in the reduced product and demonstrates the distinct phase boundaries between the Al/Fe alloy (light blue) and the Fe/Ti/Si alloy (green). A Ca/Al/Si/Mg phase (red) is also evident in the phase map. EDX spectra associated with each phase discussed can be seen in Supplementary Figures S4-S6. The composition of the Ca-rich phase in Figure 9 indicates that it could be derived from plagioclase-rich sections of the particles, as they contain the highest proportion of Ca in the starting material. However, this Ca/Si/Al phase contains a higher proportion of Ca (up to 30

wt.%) than would be expected from only reduced labradorite, indicating concentration or enrichment of Ca. Ca enrichment could potentially be due to element diffusion between adjacent phases (i.e. Ca originating from the glass *and* plagioclase phases may consolidate into a Ca/Si/Al phase seen throughout the reduced product) or because Ca from the electrolyte enters the material.

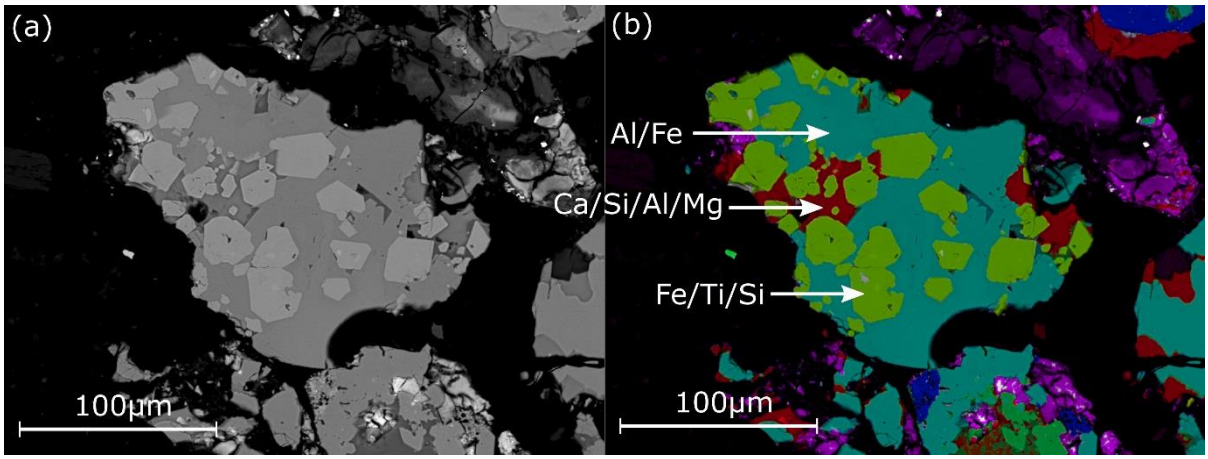

Figure 9: An example of the phase separation within individual grains showing three common phase groupings throughout the sample (4A, 950 °C, doped-SnO_2 anode, 49 hrs).

The BSE image, phase map, and elemental maps of a second reduced example are shown in Figure 10 and allow for further analysis of the alloy formation and Ca activity in the regolith simulant during the reduction. The red phase, similar to that seen in Figure 9, is composed primarily of Ca/Si/Al/Mg, while the blue phase differs only by being richer in Al and containing no Mg. The large proportion of the Mg-containing phase suggests this grain was derived from an olivine containing grain in the starting material. A Fe/Ti/Si/Al alloy (green) can be seen as a distinctly different phase inside the other alloys. As aluminium and calcium only co-appear in the JSC-2A starting material when considering only the major phases, the ratio of these elements inside a single grain can provide insight into the relative Ca content before and after reduction. In the starting material, the lowest Al to Ca wt.% ratio that could be expected based

462 on the composition of the glass in JSC-2A is 1:0.62. The inclusion of plagioclase (or even
463 pyroxene) in a grain would raise the relative proportion of Ca. The ratio in the entire reduced
464 grain area in Figure 10 is 1:0.71 Al to Ca. This falls within the range expected for the reduced
465 product of a grain containing both glass and plagioclase (or pyroxene), indicating that a
466 significant proportion of the Ca remains in the regolith simulant throughout reduction, or at
467 least a series of exchange and diffusion mechanisms with the $CaCl_2$ electrolyte leave the final
468 concentration of Ca relatively unchanged. Evidence of Ca remaining in the reduced product is
469 significant as accumulation of regolith-derived CaO in the $CaCl_2$ salt may complicate salt
470 reusability on the lunar surface due to the fact that high CaO concentrations can reduce
471 process efficiency (Chen, 2015). A detailed analysis of the behaviour of regolith-derived Ca
472 and its implications on efficiency and salt reusability is certainly required, and will be
473 conducted in future work.
474

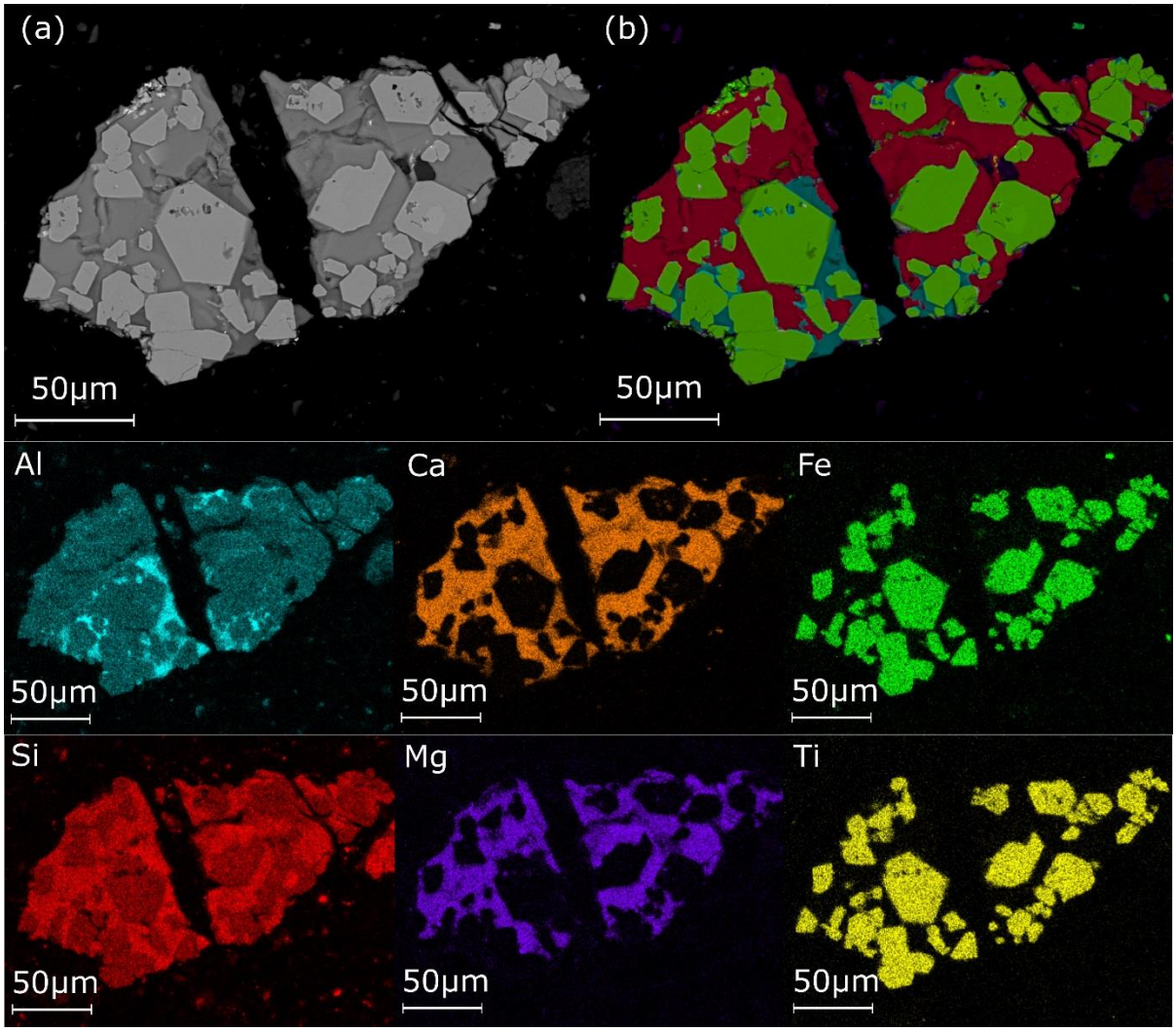

Figure 10: The BSE image, phase map, and element maps of a metallic grain in the reduced lunar simulant product (4A, 950 °C, doped-SnO_2 anode, 49 hrs).

One interesting feature that is worthy of further explanation is the apparent scarcity of specific elements in the product. Based on the SEM/EDX data, the reduced product appears to be depleted of silicon and magnesium, relative to the amount of these elements present in the starting materials. The example in Figure 10 was one of the few Si- and Mg-rich grains detected in the product, with the vast majority being dominated by the alloys of Al and Fe. Si accounts for approximately 40% of the metallic elements by weight in JSC-2A, while Al is less plentiful at ~14%. By comparison, Al and Fe are larger mass fractions than Si in almost all

reduced product grains analysed and an estimation based on low magnification EDX indicates an overall proportion of ~35% Al to only ~20% Si.

The largest proportion of Mg in the JSC-2A starting material is in olivine minerals, with an average composition of $Mg_{1.44}Fe_{0.56}SiO_4$. Figure 11 shows the phase map of a grain from a partial reduction experiment that almost certainly contained olivine based on the chemistry, which helps to give some insight into the reduction mechanism of this mineral. It appears that Fe-rich metallic blebs, composed of the elements that are the easiest to reduce, form within olivine-rich particles when these are exposed to the reducing environment (phase depicted as green in Figure 11). The remaining elements then separate into two distinct phases, a partially reduced phase consisting primarily of Si/Ca (along with some Mg; the red phase in Figure 11), while the majority of the Mg forms a separate phase of pure, unreduced MgO (shown as the purple phase in Figure 11). This separation is likely due to MgO being one of the hardest, and therefore last, oxides to reduce. EDX spectra associated with each phase discussed can be seen in Supplementary Figures S11-S14. It is interesting to note the inclusion of Ca in partially reduced phases, as this does not originate from the olivine. As Al is also seen in the metallic blebs, this could have originated from adjacent glass or plagioclase phases. Alternatively, Ca may be incorporated into the lattice structure as an intermediate, as is the case in the reduction mechanism of pure TiO_2 (Benson, 2016). An in-depth study into the reduction mechanism of individual minerals and phases would be required to confirm this mechanism.

Several possibilities exist for the fate of the Mg in the MgO phase upon reduction, considering the apparent depletion of Mg in the product. Firstly, it is plausible that Mg could enter the

electrolyte as MgO or $MgCl_2$, however, ICP-MS analysis of the $CaCl_2$ electrolyte proved this not to be the case, actually showing a lower concentration of Mg at the end of the reduction experiment (37 vs. 69 ppm). Alternatively, all the Mg could remain in the product as variations of the Ca/Si/Al/Mg alloy observed. While the frequency and composition of these phases identified in the reduced product do not support this hypothesis, the apparent depletion in Mg may just be a chance result of the SEM/EDX analysis, as it is not a bulk analytical technique. A third possibility identified is that reduction of the pure MgO phase seen in Figure 11 could form Mg metal, which has a melting point of 650 °C and a density significantly lower than that of $CaCl_2$. As such, droplets of liquid Mg may leave the cathode material and float to the top of the reactor, possibly within a protective shell of MgO. It is possible that in a similar mechanism, silicon forms an alloy that leaves the cathode basket and agglomerates at an electrolyte interface, thus leaving the reduced solid product depleted of this element. If these processes were confirmed and understood, then in a larger-scale reduction, specific metals and alloys could potentially be separated and siphoned off during electrolysis. Further work to confirm this hypothesis is required.

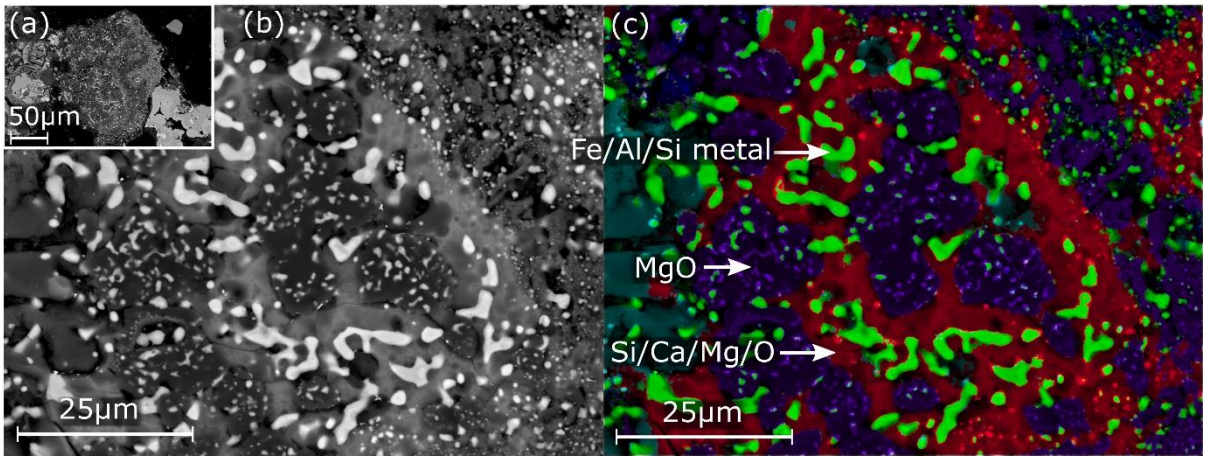

Figure 11: A partially reduced olivine-rich grain, (a) shows the overall grain, (b) and (c) show the magnified BSE and phase map images respectively (4A, 950 °C, doped-SnO_2 anode, 26 hrs).

There was no evidence of Na or K in the reduced product, whereas these oxides together account for 3-4% by weight of the simulant starting material. ICP-MS analysis of the electrolyte before and after the reduction shows increases in Na and K approximately equivalent to the total amount of these elements in the starting material, suggesting that both have dissolved into the electrolyte as oxides or chlorides. The exact process of dissolution will likely need to be addressed further when considering salt reusability, especially when using terrestrial materials that have a larger proportion of alkali metals. Interestingly, as these are elements are known to be depleted in the lunar crust, this process actually makes the metallic product of the reduction more similar in elemental composition to that which might be expected from the reduction of genuine lunar regolith.

There was evidence of anode-derived Sn in the product, seen in the EDX spectra in Supplementary Figure S6. This Sn impurity was often evident on the external edges of grains, suggesting Sn plating during the reduction process. Minimisation of anode corrosion through control of processing parameters will prevent Sn from entering the electrolyte and plating on the cathodic surfaces. The optimisation of the reduction time and charge passed will be addressed in future work. Ni and Cr impurities originating from the SS cathode basket were also identified by EDX. With future experiments that eliminate the SS mesh, we hope to simultaneously eliminate this source of impurity, and eliminate the need for sieving the

550 regolith simulant starting material to a specified grain size. Such an experimental adaptation
551 will be advantageous in terms of removing a challenging beneficiation step and utilising the
552 majority of excavated material on the lunar surface.

553

554 Overall, the characterisation of the metallic material shows a surprising consistency in the
555 alloy mixtures present. The composition of the phases in the reduced material clearly shows
556 that it is not a simple phase-to-phase reduction (i.e. the glass phase does not simply form a
557 metallic slag of the elements in the original glass), but rather elemental diffusion in the solid-
558 state forms specific alloys based on the ease with which elements are reduced and the affinity
559 of various metals for forming alloys together. A complete understanding of this formation
560 process, and the influence of the feedstock composition and process parameters, has the
561 potential to allow for the formation and separation of useful alloys from unbeneficiated lunar
562 regolith.

563

564

565 **4. Conclusions**

566 These preliminary results provide a proof-of-concept for the reduction of lunar regolith
567 simulants by the Metalysis-FFC process to extract oxygen and produce metals and alloys as
568 by-products. We have shown that JSC-2A lunar regolith simulant can be reduced by molten
569 salt electrolysis at ~950 °C until it is essentially metallic (96% of the total oxygen removed).
570 This demonstrates that, with appropriate adaptions, close to 100% oxygen recovery from
571 lunar regolith is possible using the Metalysis-FFC process, which would give a potential oxygen
572 yield of 40-45 wt.% for every kg of regolith excavated, dependent on location. A reasonable

quantity of the oxygen extracted was detected as O_2 gas, and we believe it should be possible to isolate and quantify much more of this O_2 gas with some modifications to the apparatus. Whilst the production of oxygen was a clear indication that the SnO_2 anode was competent for this reaction, anode re-use was hampered by both mechanical and chemical issues that will be addressed in future work. Characterisation of the alloys produced shows that three distinct alloy groups dominate the product:

- An Al/Fe alloy (sometimes with the inclusion of Si)
- A Fe/Si alloy (sometimes with the inclusion of Ti and/or Al)
- A Ca/Si/Al alloy (sometimes with the inclusion of Mg)

This is the first successful demonstration of solid-state powder-to-powder regolith simulant processing that yields metal alloys as products. Furthermore, the clear separation of various alloy phases, and the apparent depletion of other metallic components, introduces the exciting potential for metal/alloy separation and refining from unbeneficiated lunar regolith. Additionally, there exists the potential to use a beneficiated feedstock to produce specifically designed alloys. The production of useful metals as a by-product of this oxygen extraction technique means that the Metalysis-FFC process could still hold great value even if polar ice is found to be a viable and plentiful resource for oxygen production.

At this preliminary stage in the project, optimisation of the experimental set-up and parameters are yet to be addressed. It is expected that significant improvements to the efficiency of the process with respect to reduction time and energy consumption will be possible. For example, we intend to identify a point at which partial reduction of regolith yields the maximum amount of oxygen for the lowest energy input, whilst still yielding a semi-

metallic product that can be utilised in lunar infrastructure. Current engineering for the Metalysis Generation 1 R&D cells (the scale used in the present study) is specific for a laboratory environment where observation and data collection are the driver; re-engineering the cell will give the opportunity to use different materials to improve heat retention and implement new solutions, such as internal heating, to make the system more energy efficient. Regardless, this approach is full of promise, as there seems to be no fundamental reason as to why this process should not operate effectively with lunar regolith. We believe that the utilisation of the Metalysis-FFC process, applying the developments implemented in the past decade, offers an exciting alternative to other technologies for oxygen production on the lunar surface.

5. Acknowledgments

This project is jointly funded by ESA, Metalysis, and the University of Glasgow through the ESA Networking/Partnership Initiative (NPI 599 – 2018). MDS thanks the Royal Society for a University Research Fellowship (UF150104). We thank Dr Aidan Cowley (European Astronaut Centre, Cologne) for supplying samples of JSC-2A. We acknowledge Claire Seddon, Joe Hardman, Sarah Boot, and Basharat Ali (Metalysis Ltd.) for assistance with the electrochemical experiments and product characterisation; and Peter Chung, James Gallagher (University of Glasgow), and Dr Jim Buckman (Heriot-Watt University) for their helpful facilitation of the SEM/EDX analysis. The data underpinning this work are available by contacting the authors.

6. Declaration of Interests

Dr Melchiorri Conti and Dr Nader Khan are employees at Metalysis Ltd.

7. References

Allen, C.C., Morris, R.V. and McKay, D.S., 1996. Oxygen extraction from lunar soils and pyroclastic glass. *Journal of Geophysical Research: Planets*, *101*(E11), pp.26085-26095.

Anand, M., Crawford, I.A., Balat-Pichelin, M., Abanades, S., van Westrenen, W., Péraudeau, G., Jaumann, R., Seboldt, W. 2012. A brief review of chemical and mineralogical resources on the Moon and likely initial in situ resource utilization (ISRU) applications. *Planetary and Space Science* 74, 42-48.

Balasubramaniam, R., Gokoglu, S. and Hegde, U., 2010. The reduction of lunar regolith by carbothermal processing using methane. *International Journal of Mineral Processing*, *96*(1-4), pp.54-61.

Benson, L.L., Mellor, I. and Jackson, M., 2016. Direct reduction of synthetic rutile using the FFC process to produce low-cost novel titanium alloys. *Journal of Materials Science*, *51*(9), pp.4250-4261.

Canup, R.M., Visscher, C., Salmon, J. and Fegley Jr, B., 2015. Lunar volatile depletion due to incomplete accretion within an impact-generated disk. *Nature Geoscience*, *8*(12), p.918.

Carpenter, J., Fisackerly, R. and Houdou, B., 2016. Establishing lunar resource viability. *Space Policy*, *37*, pp.52-57.

Chen, G. Z., Fray, D. J., Farthing, T. W. 2000. Direct electrochemical reduction of titanium dioxide to titanium in molten calcium chloride. *Nature* 407, 361–364.

643 Chen, G.Z., 2015. The FFC Cambridge process and its relevance to valorisation of
644 ilmenite and titanium-rich slag. *Mineral Processing and Extractive Metallurgy*, *124*(2), pp.96-
645 105.
646 Colson, R.O., Haskin, L.A., 1992. Oxygen from the lunar soil by molten silicate
647 electrolysis. In: McKay, F.A., McKay, D.S., Duke, M.B. (Eds.*), Space Resources, Vol. 3. Materials*,
648 NASA, Lyndon B Johnson Space Center, Houston, TX, pp. 195–209.
649 Colson, R.O., Haskin, L.A., 1993. Producing oxygen by silicate melt electrolysis. In:
650 Lewis, J., Matthews, M.S., Guerrieri, M.L. (Eds.), *Resources of Near-Earth Space*. University of
651 Arizona Press, Tucson, AZ, pp. 109–127.
652 Crawford, I.A., 2015. Lunar resources: A review. *Progress in Physical Geography*, *39*(2),
653 pp.137-167.
654 Ellis, M.B.D. and Doughty, G.R., 2017. Solid State Manufacture of High Entropy Alloys-
655 Preliminary Studies. *MRS Advances*, *2*(26), pp.1375-1380.
656 Fray, D.J., Farthing, T.W, Chen, Z., 1999. Removal of oxygen from metal oxides and
657 solid solutions by electrolysis in a fused salt. WO/99/64638.
658 Friedlander, H.N., 1985. An analysis of alternate hydrogen sources for lunar
659 manufacture. In: Mendell, W.W. (Eds.), *Lunar Bases and Space Activities of the 21st Century.*
660 Lunar and Planetary Institute, Houston, pp. 611-618.
661 Gibson, M.A., Knudsen, C.W., Brueneman, D.J., Allen, C.C., Kanamori, H., McKay, D.S.,
662 1994. Reduction of lunar basalt 70035: oxygen yield and reaction product analysis. *Journal of*
663 *Geophysical Research* 99, 10887–10897.
664 Gustafson, R.J., Rice, E.E., White, B.C., 2005. Carbon reduction of lunar regolith for
665 oxygen production. *AIP Conference Proceedings* 746, 1224–1228.

Hasnain, S.M., 1998. Review on sustainable thermal energy storage technologies, Part I: heat storage materials and techniques. *Energy conversion and management*, *39*(11), pp.1127-1138.

Hill, E., Mellin, M.J., Deane, B., Liu, Y. and Taylor, L.A., 2007. Apollo sample 70051 and high-and low-Ti lunar soil simulants MLS-1A and JSC-1A: Implications for future lunar exploration. *Journal of Geophysical Research: Planets*, *112*(E2).

Jiao, S.Q., Fray, D.J., 2010. Development of an inert anode for electrowinning in calcium chloride-calcium oxide melts. *Metallurgical and Materials Transactions B* 41, 74–79.

Jiao, S.Q., Kumar, K.N.P., Kilby, K.T., Fray, D.J., 2009. Preparation and electrical properties of *x* $CaRuO_3$/(1−x) $CaTiO_3$ perovskite composites. *Materials Research Bulletin* 44, 1738–1742.

Kesterke, D.G., 1970. "Electrowinning oxygen from silicate rocks." NASA Special Publication 229: 139.

Kilby, K.T., Jiao, S.Q., Fray, D.J., 2010. Current efficiency studies for graphite and SnO_2-based anodes for the electro-deoxidation of metal oxides. *Electrochimica Acta* 55, 7126–7133.

Li, S., Lucey, P.G., Milliken, R.E., Hayne, P.O., Fisher, E., Williams, J.P., Hurley, D.M. and Elphic, R.C., 2018. Direct evidence of surface exposed water ice in the lunar polar regions. *Proceedings of the National Academy of Sciences*, *115*(36), pp.8907-8912.

Li, Y., Li, X., Wang, S., Tang, H., Gan, H., Li, S., Wei, G., Zheng, Y., Tsang, K.T. and Ouyang, Z., 2012. In-situ water production by reducing ilmenite. In: Badescu, V. (Ed.), *Moon,* Springer, Berlin, Heidelberg, pp. 189-200.

688 Liu, A., Shi, Z., Hu, X., Gao, B. and Wang, Z., 2017. Lunar Soil Simulant Electrolysis Using
689 Inert Anode for Al-Si Alloy and Oxygen Production. *Journal of The Electrochemical*
690 *Society*, 164(2), pp.H126-H133.
691 McKay, D.S., Heiken, G., Basu, A., Blanford, G., Simon, S., Reedy, R., French, B.M. and
692 Papike, J., 1991. The lunar regolith. In Heiken, G.H., Vaniman, D.T. and French, B.M. (Eds.),
693 *Lunar sourcebook*, Cambridge University Press, pp.285-356.
694 Mellor, I. and Doughty, G., 2016. Novel and emerging routes for titanium powder
695 production-an overview. *Key Engineering Materials*, *704*, p.271.
696 Papike, J., Taylor, L. and Simon, S., 1991. Lunar minerals. In: Heiken, G.H., Vaniman,
697 D.T. and French, B.M. (Eds.), *Lunar sourcebook*, , Cambridge University Press, pp.121-181.
698 Ray, C.S., Reis, S.T., Sen, S. and O'Dell, J.S., 2010. JSC-1A lunar soil simulant:
699 Characterization, glass formation, and selected glass properties. *Journal of Non-Crystalline*
700 *Solids*, *356*(44-49), pp.2369-2374.
701 Rosenberg, S.D., Beegle Jr., R.L., Guter, G.A., Miller, F.E., Rothenberg, M., 1992. The
702 onsite manufacture of propellant oxygen from lunar resources. In: McKay, F.A., McKay, D.S,
703 Duke, M.B. (Eds.), *Space Resources, Vol. 3. Materials,* NASA, Lyndon B Johnson Space Center,
704 Houston, TX, pp. 162–185.
705 Sanders, G.B. and Larson, W.E., 2012. Progress Made in Lunar In Situ Resource
706 Utilization under NASA's Exploration Technology and Development Program. *Journal of*
707 *Aerospace Engineering*, *26*(1), pp.5-17.
708 Schreiner, S.S., Sibille, L., Dominguez, J.A. and Hoffman, J.A., 2016. A parametric sizing
709 model for Molten Regolith Electrolysis reactors to produce oxygen on the Moon. *Advances in*
710 *Space Research*, *57*(7), pp.1585-1603.

711 Schrunk, D., Sharpe, B., Cooper, B.L. and Thangavelu, M., 2007. *The Moon: Resources,*
712 *future development and settlement*. Springer Science & Business Media.
713 Schwandt, C., Doughty, G.R. and Fray, D.J., 2010. The FFC-Cambridge process for
714 titanium metal winning. *Key Engineering Materials*, Vol. 436, pp. 13-25.
715 Schwandt, C., Hamilton, J. A., Fray, D. J., Crawford, I. A. 2012a. The production of
716 oxygen and metal from lunar regolith. *Planetary and Space Science* 74, 49–56.
717 Schwandt, C., Hamilton, J.A., Fray, D.J. and Crawford, I.A., 2012b. Oxygen from lunar
718 regolith. In: Badescu, V. (Ed.), *Moon*. Springer, Berlin, Heidelberg, pp. 165-187.
719 Sirk, A.H., Sadoway, D.R. and Sibille, L., 2010. Direct electrolysis of molten lunar
720 regolith for the production of oxygen and metals on the moon. *ECS Transactions*, *28*(6),
721 pp.367-373.
722 Taylor, L.A., Carrier, W.D., 1993. Oxygen production on the Moon: an overview and
723 evaluation. In: Lewis, J., Matthews, M.S., Guerrieri, M.L. (Eds.), *Resources of Near-Earth Space*.
724 University of Arizona Press, Tucson, AZ, pp. 69–108.
725 Taylor, L.A., Pieters, C.M. and Britt, D., 2016. Evaluations of lunar regolith
726 simulants. *Planetary and Space Science*, *126*, pp.1-7.
727 Vai, A. T., Yurko, J. A., Wang, D. H., and Sadoway, D. R., 2010. Molten oxide electrolysis
728 for lunar oxygen generation using in-situ resources. *Jim Evans Honorary Symposium, The*
729 *Minerals, Metals & Materials Society (TMS) Annual Meeting 2010*, Minerals, Metals &
730 Materials Society, Warrendale, PA, pp.301-308.
731 Vaughan, D. and Conti, M. (Metalysis Ltd), 2017. Manufacturing apparatus and
732 method. WO/2017/203245.

733 Wang, D., Gmitter, A.J. and Sadoway, D.R., 2011. Production of oxygen gas and liquid
734 metal by electrochemical decomposition of molten iron oxide. *Journal of The Electrochemical*
735 *Society*, 158(6), pp.E51-E54.
736

Appendix with Supplementary Figures

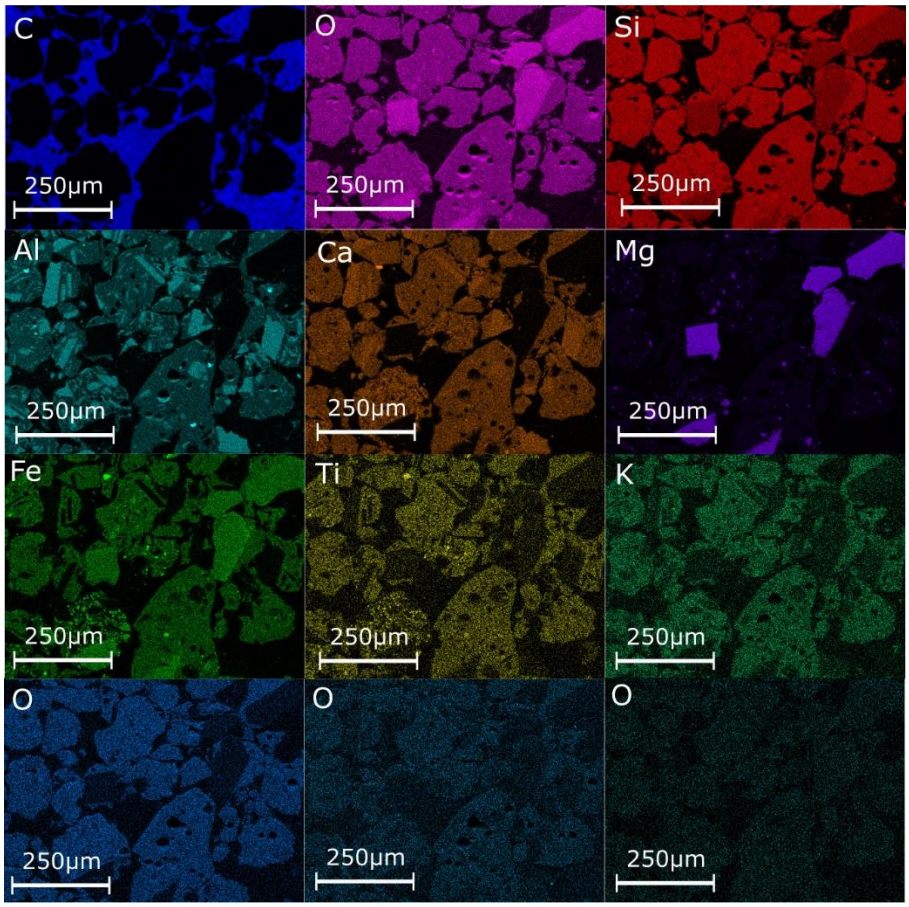

Figure S1: EDX element maps of JSC-2A (>53 µm).

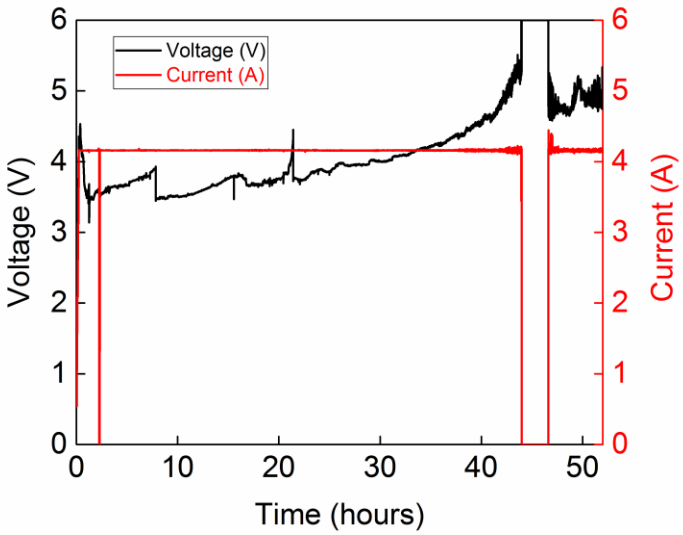

Figure S2: Current and potential vs. time graph for the reduction corresponding to the oxygen removal graph shown in Figure 6.

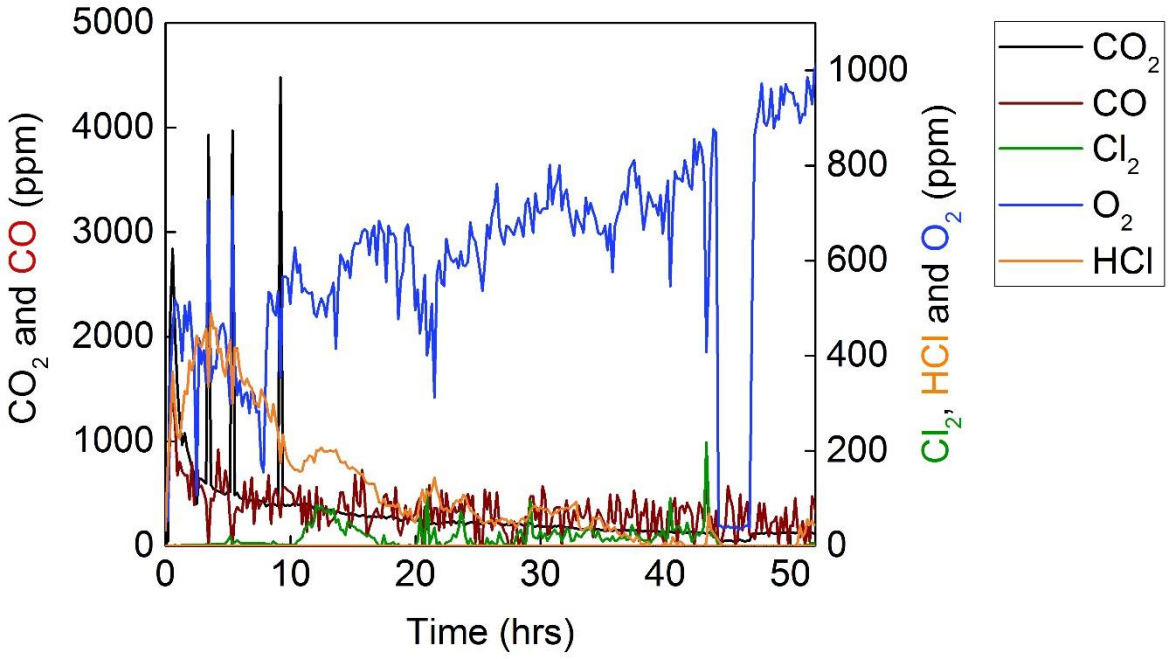

743

744 **Figure S3:** The mass spectrometry data corresponding to the oxygen removal graph shown in

745 Figure 6.

746

747 **Figures S4 – S14** give the EDX spectra corresponding to the phases discussed. Where possible,

748 EDX spot measurements taken away from any inclusions or neighbouring phases were used

749 to give a more accurate representation of the phase chemistry.

750

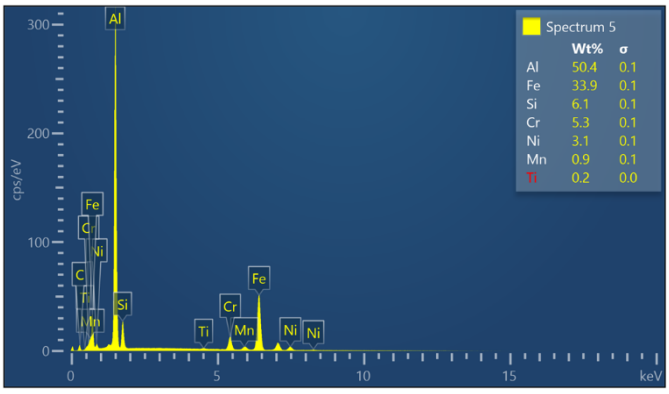

751

752 **Figure S4:** EDX spectrum corresponding to the light blue phase in Figure 9 showing it to be an

753 alloy of primarily Al and Fe.

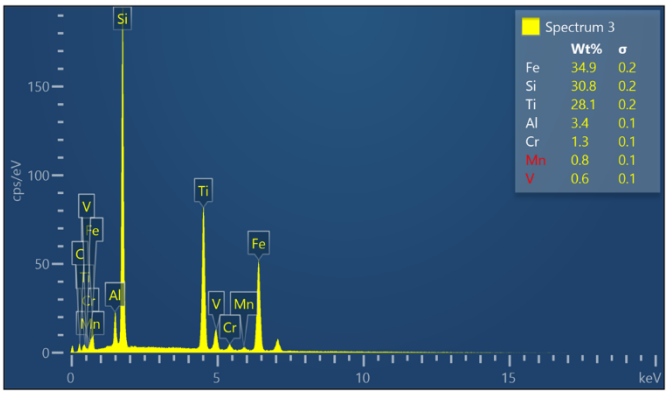

Figure S5: EDX spectrum corresponding to the green phase in Figure 9 showing it to be an alloy of primarily Fe, Si and Ti.

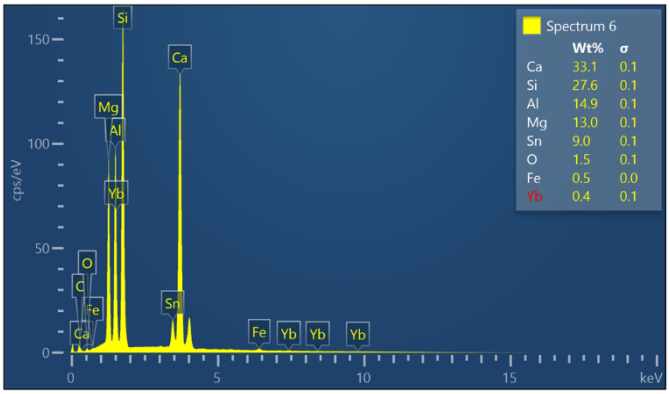

Figure S6: EDX spectrum corresponding to the red phase in Figure 9 showing it to be an alloy of primarily Ca, Si, Al, and Mg.

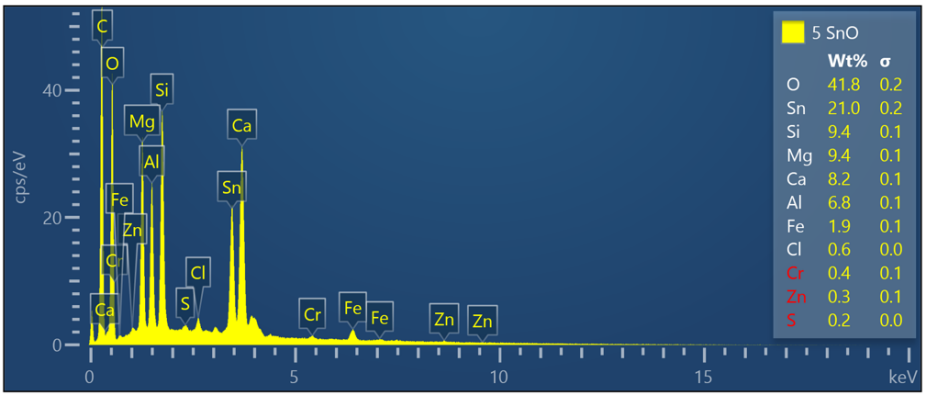

Figure S7: EDX spectrum corresponding to the purple phase in Figure 9 showing it to be an alloy of primarily Sn and O.

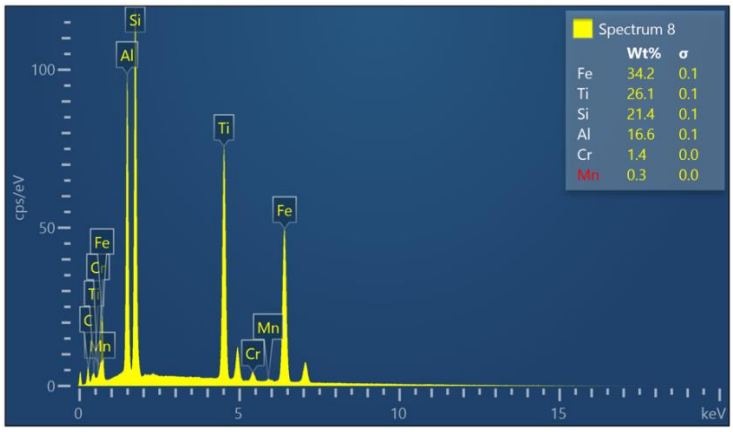

763

764 **Figure S8:** EDX spectrum corresponding to the green phase in Figure 10 showing it to consist

765 primarily of Fe, Si, Ti, and Al.

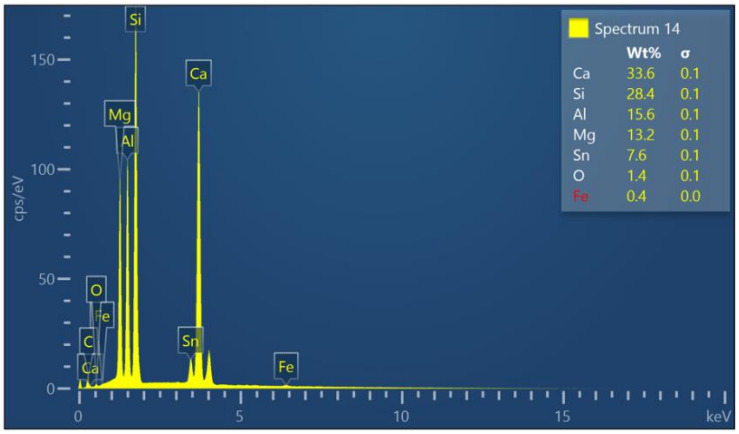

766

767 **Figure S9:** EDX spectrum corresponding to the red phase in Figure 10 showing it to consist

768 primarily of Ca, Si, Al, and Mg.

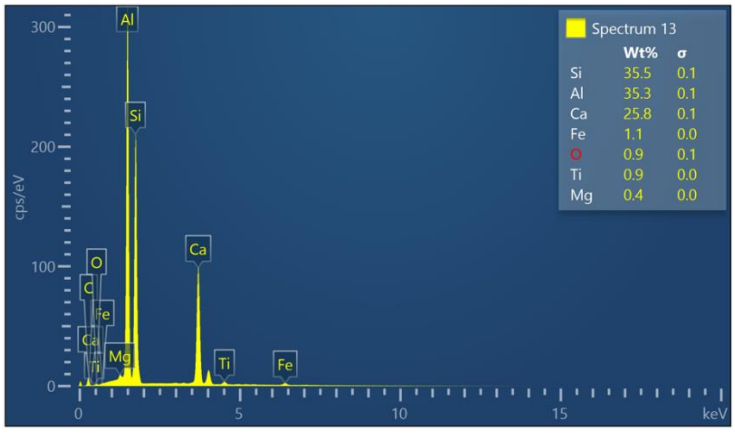

769

770 **Figure S10:** EDX spectrum corresponding to the blue phase in Figure 10 showing it to consist

771 primarily of Si, Al, and Ca.

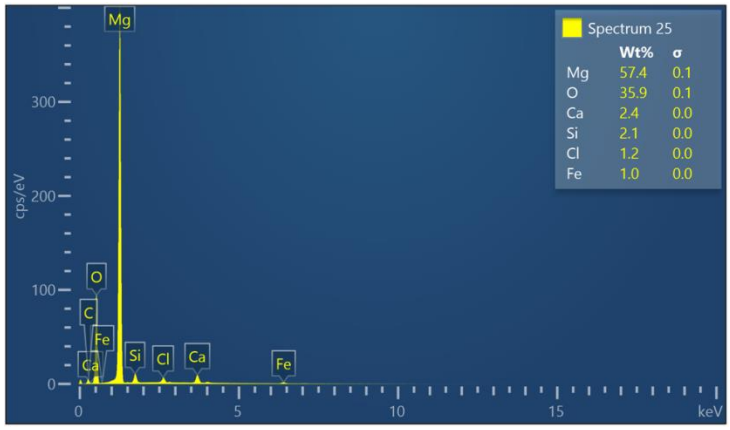

772

773 **Figure S11:** EDX spectrum corresponding to the purple phase in Figure 11 showing it to consist

774 primarily of MgO.

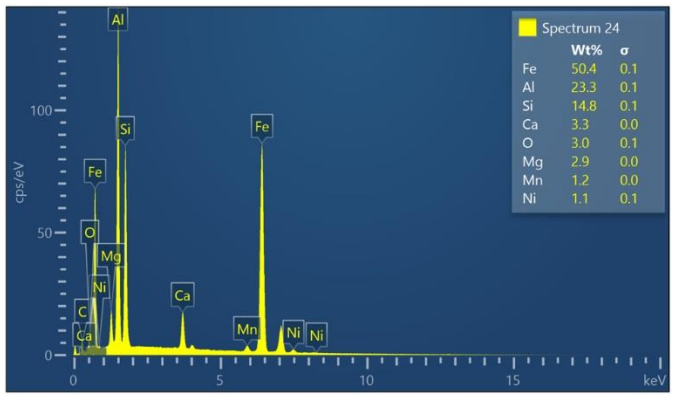

775

776 **Figure S12:** EDX spectrum corresponding to the green phase in Figure 11 showing it to consist

777 primarily of Fe, Al, and Si.

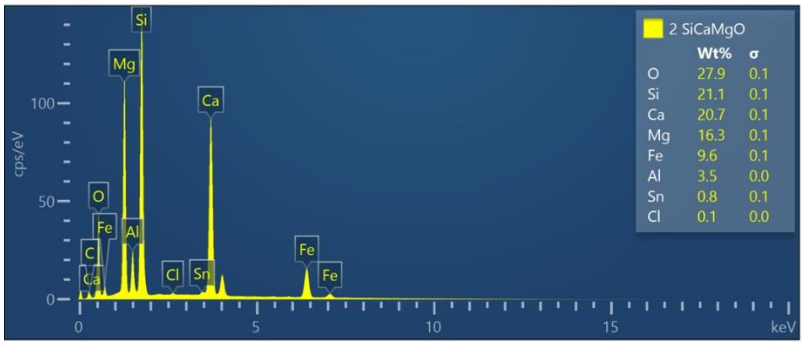

778

779 **Figure S13:** EDX spectrum corresponding to the red phase in Figure 11 showing it to consist

780 primarily of Si, Ca, Mg, and O.

781 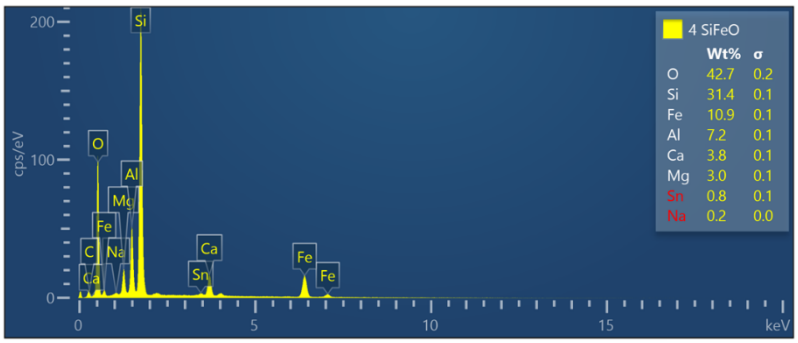

782 **Figure S14:** EDX spectrum corresponding to the blue phase in Figure 11 showing it to consist

783 primarily of Si, Fe, Al, and O.

784

785

786

787